THE TRANSFORMATION OF DEEP WATER WAVE HINDCASTS TO SHALLOW WATER

Claudio Fassardi

BMT Scientific Marine Services Inc
Escondido, California, USA

1. INTRODUCTION

The definition of wave conditions in shallow water is an essential aspect in the design and operation of a wide variety of coastal facilities and for the safe performance of human activities in coastal areas. Port developments, marine terminals, coastal management strategies, downtime analysis of vessel activities, etc. are a few examples for which the assessment of wave conditions is important.

Engineers are usually confronted with insufficient or no wave data when performing studies in remote or under developed coastal areas. Measurements at the site of interest would be the most adequate source of data, but these are often expensive and may not produce sufficient data to allow, for example, the computation of extreme wave conditions or include the long-term variability of the wave climate. In the absence of measured data, the standard practice is the use of wave hindcasts.

Ideally, such wave hindcasts should capture the "basin" scale events, so that the impact of long period swell generated by distant storms could be accounted for. At the same time, such a hindcast should include the local short period wind waves. Finally, it would be desirable for the hindcast to include the effects of the wave transformation processes such as diffraction, shoaling, refraction and wave breaking due to the features of the bathymetry and presence of islands, headlands and shoals. The computation of site-specific long-term wave hindcasts with these requirements is possible but with caveats and, for many projects, it often constitutes an expensive or impractical alternative.

This paper describes a methodology to derive shallow water wave hindcasts from deep water wave hindcasts that accounts for "basin" and local scale events. Through a combination of wave transformation modeling and data fitting techniques, transfer functions between the deep water wave conditions and those at a location of interest in shallow water are derived. Assuming linear wave theory, these transfer functions account for the dependency of shallow water waves on deep water wave height, period, direction, water level and the particular features in the vicinity of the site of interest such as bathymetry, islands, headlands and structures.

An example of the application of this method is presented for Imperial Beach, California. For the period of 1983 to 1996, a comparison between derived and measured wave parameters is presented. In addition, the sensitivity of the inclusion of water level changes in the derived shallow water hindcast is discussed.

2. METHODOLOGY

As they propagate from deep to shallow water, waves experience changes in height and direction due to the presence of uneven bathymetry, islands, headlands and structures. The wave transformation processes comprise shoaling, refraction, diffraction, wave breaking, friction, etc. which will change the waves height and direction but would leave the wave period unchanged.

Shoaling, refraction and diffraction are phenomena that have been approached and studied as linear problems and are resolved in the same manner by numerical models. In this approach, the resulting shallow water wave height at a point of interest after the wave transformation process has taken place is assumed to be linearly proportional to the deep water wave height. This is an important consideration because it allows one to model, for a given pair of deep water wave period and direction, the wave transformation process using a unit deep water wave height (i.e. H = 1) and using the resulting shallow water wave height as a "wave transformation coefficient" (Ct) that accounts for the effect of shoaling (Cs), refraction (Cr) and diffraction (Cd); (i.e. Ct = Cs x Cr x Cd). However, the use of H = 1 as input limits the methodology to the study of areas where wave breaking is not important. If the effect of water level variations is important, the wave transformation process could be modeled for different water levels and therefore Ct could be expressed as:

$$Ct = f(T, WD_{deep\ water}, \text{Water Level}) \qquad (1)$$

where T is the wave period and WD is the wave direction. The shallow water wave height at a point of interest, that results from a given set of deep water

wave height, period, direction and water level can be computed simply by:

$$H_{shallow\ water} = H_{deep\ water} \times Ct \quad (2)$$

The shallow water wave direction is independent of wave height and dependent on deep water wave period and direction, and water level. It could be expressed as:

$$WD_{shallow\ water} = f(T, WD_{deep\ water}, \text{Water Level}) \quad (3)$$

In linear wave theory, the wave transformation processes will change the waves height and direction but would leave the wave period unchanged. Therefore,

$$T_{shallow\ water} = T_{deep\ water} \quad (4)$$

In order to compute a shallow water hindcast at a particular location, it would be desirable to transform through modeling every wave condition in the deep water wave hindcast. However, the amount of data in the hindcast may make this approach very time consuming and impractical. Using the dependency of the shallow water wave conditions on the deep water wave height, period and direction, and water level (Eqs. (1) through (4)) the wave conditions at the location of interest can be computed in the following manner:

1. A Frequency of Occurrence (or Probability) Table of wave periods and directions is computed from the deep water wave hindcast and a matrix covering the range of most likely periods and directions is defined. Similarly, water levels at the location of interest are examined to define the maximum, minimum and mean water levels.
2. Pairs of deep water wave periods and directions are selected from the matrix and used with a unit wave height (H = 1) to compute, with a wave transformation model, wave heights (Ct's) and directions at the location of interest, for the water levels selected.
3. Three-dimensional Ct and wave direction transfer functions are derived using B-splines, a technique that provides continuous and accurate representations of the data. The significant advantage of B-splines over other methods of fitting data is that the functional form of the data does not need to be known beforehand and it does not produce undesirable wiggles away from data points which is often typical, for example, with polynomial fits.
4. The Ct and wave direction transfer functions are used to derive the wave conditions at the point of interest in shallow water, by operating on the deep water wave hindcast at each time interval.

The computation of shallow water seas and swell hindcasts may be required when the effects of these two different wave systems are important for the problem to be studied. In these cases, provided that the deep water seas and swell hindcasts are available, these can be computed independently by applying steps 1) through 4). A "total wave" height hindcast can be computed, for each time interval, from the seas and swell shallow water hindcasts according to:

$$H_{total} = (H_{swell}^2 + H_{seas}^2)^{1/2} \quad (5)$$

The dominant period would be defined as the one corresponding to the greater of the swell or seas height. For instance, if $H_{swell} > H_{seas}$ then the dominant period would correspond to the swell period. The dominant direction could be computed similarly.

3. CASE STUDY - OVERVIEW

An application of the method is presented for Imperial Beach, California, for which wave records are available for the period 1983 to 1996. Measurements were performed by the Scripps Institution of Oceanography (SIO) through the Coastal Data Information Program (CDIP) with a pressure sensor array located in approximately 10.4 m (MLLW) water depth.

GROW (Global Re-analysis of Offshore Winds), a wave hindcast developed by Oceanweather, Inc. was used in this study. The hindcast includes wave parameters partitioned in seas and swell, every three hours, and basin and local scale events. The wave hindcast used as input corresponded to station 38023. Additonal information about GROW can be found in GROW's Project Description document.

The wave transformation model used in this study was MIKE 21 Parabolic Mild Slope (PMS), developed by the Danish Hydraulic Institute (DHI). It accounts for refraction, shoaling and diffraction of linear water waves propagating on gently sloping bathymetry. Upon evaluation of the offshore area it was determined that MIKE 21 PMS was a suitable model to take into account the effect of the Coronado Islands just offshore Imperial Beach, local submarine ridges, canyons and shoals.

4. MODEL SETUP

4.1. Wave Conditions

The deep water wave conditions matrices, characterized by peak period (Tp) and mean wave direction (MWD), for input in the wave transformation modeling were defined for seas and swell by inspection of the corresponding frequency of occurrence tables derived from the GROW hindcast. The ranges of deep water wave periods and directions were selected to cover the range of likely wave conditions (i.e . probability greater than 80%).

The wave conditions (pairs of Tp and MWD) selected for modeling are summarized in Table 1.

	Tp	MWD
Seas	5 to 9 seconds, every 1 second	250˚ to 320˚, every 10˚
Swell	10 to 22 seconds, every 2 seconds	210˚ to 310˚, every 10˚

Table 1. Deep water wave conditions used for modeling.

Waves with periods of Tp = 2 to 4 seconds are expected to occur under the typical seabreeze conditions. However, wave conditions within this range of periods were not modeled because the selected grid model spacing ($\Delta x = \Delta y = 10$ m) would not allow the adequate resolution of these waves. The grid spacing was selected based on a trade off between extent of area to cover, computational resources and resolution of short period waves.

Seas were modeled with a Pierson-Moskowitz spectrum and swell with a Jonswap spectrum with a peak enhancement factor, γ, of 9. These selections were based on experience from similar studies and are consistent with recommendations by Goda (1985).

Directional spreading was modeled using the following cosine power function:

$$G(\theta) = G_0 \cos^n(\theta - \theta_{mean}) \quad (6)$$

where G_0 is the normalizing function, θ_{mean} is the mean wave direction (MWD) and n is the directional spreading index. The relationship between the angular spreading in the GROW hindcast (ANGSPR) and n is as follows:

$$n = (2*ANGSPR) / (1 - ANGSPR) \quad (7)$$

The directional spreading index n for seas and swell was derived in the following manner. The GROW wave hindcast reports the angular spreading *ANGSPR* for the total seas. Since the angular spreading was needed for the seas and swell independently, the hindcast was sorted so that "seas only" and "swell only" cases could be isolated. Average values of *ANGSPR* were computed and corresponding n's were derived according to Eq. (7). Inman (1974) concluded that an expected directional variability of energy of +/- 15˚ is appropriate for northern hemisphere storms in the Pacific Ocean. Arthur (1951) estimated the directional variability of the southern swell to be approximately +/- 5˚. Table 2 summarizes the values for directional spreading index, maximum directional deviation from the mean direction and number of discrete directions adopted for seas and swell.

	Seas	Swell
Directional Spreading Index, *n*	12	23
Max. Directional Deviation	+/- 45˚	+/- 15˚
Number of Discrete Directions	7	5

Table 2. Directional spreading parameters for seas and swell.

Note in Table 2 the relatively high value $n = 12$ for seas. It was not possible to isolate pure seas completely since at Imperial Beach, there is always the presence of swell. Therefore, a low threshold of swell height equal to 0.25 m was selected to gather "almost pure" seas and derive the corresponding n.

The numerical model used in the study was MIKE 21 PMS. This model is based on a parabolic approximation to the elliptic mild-slope equation governing the refraction, shoaling and diffraction of linear water waves propagating on gently sloping bathymetry. The model uses a finite difference scheme to solve the equations and requires as input a rectangular bathymetry grid covering the area of interest. The parabolic approximation is obtained by assuming a principal wave direction which is parallel to the "x" direction of the model grid. Improvements implemented in MIKE 21 PMS have permitted the use of the parabolic approximation for waves propagating at relatively large angles (relative to the "x" axis). The "wave" boundary is the "y" axis. An additional feature of the model is the ability to simulate directional and frequency spreading of the propagating waves by the use of linear superposition.

Given the wide range of deep water wave directions to be modeled three model grids were developed with a square grid spacing of $\Delta x = \Delta y = 10$ m. Table 3 summarizes the grid usage scheme. Figure 1 shows the three wave modeling grids used, the approximate location of the CDIP pressure sensor array and the GROW (38023) grid point. The double lines indicate the incident wave boundaries for each grid. The model bathymetry was referred to the MLLW datum.

"x" Axis Direction	Seas Directions	Swell Directions
230˚	250˚	210˚ to 250˚
270˚	260˚ to 280˚	260˚ to 280˚
305˚	290˚ to 320˚	290˚ to 310˚

Table 3. Wave modeling grids usage scheme.

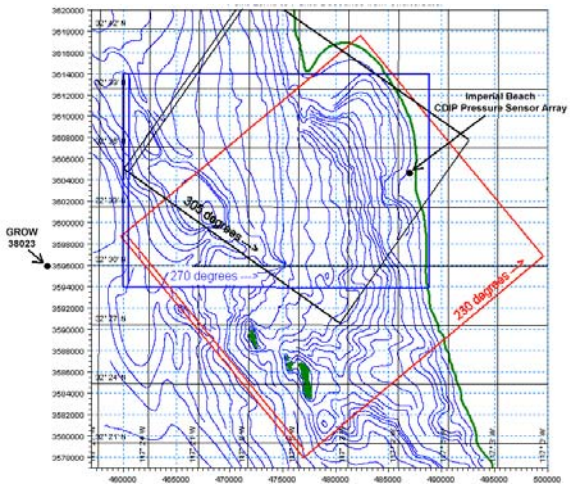

Figure 1. CDIP pressure sensor array and GROW grid point locations, and wave model grids (double lines = incident wave boundary).

4.2. CDIP Wave Data

The CDIP wave data was downloaded from http://cdip.ucsd.edu/. The data used in this study corresponded to station 055, denominated Imperial Beach North. Measurements at this station were performed with a pressure sensor array located in approximately 10 m water depth (MLLW) at 32° 35' N 117° 8.20' W. The station was commissioned in July of 1983 and decommissioned in December of 1996. Data from this station consisted of date and time (UTC), significant wave height, peak period, mean direction, depth and average period. CDIP derived the water surface elevation from the pressure measurements applying the Linear Wave Theory transfer function. Additional information about the instruments, data acquisition, analysis and management can be found at CDIP's website.

4.3. Bathymetry

The offshore bathymetry was obtained from charts by Continental Shelf Data Systems in 1971. These charts were produced from data in U.S. Government original manuscripts of hydrographic surveys and published nautical charts. The model bathymetry was referred to the MLLW.

4.4. Water Levels

For each of the wave conditions summarized in Table 1 wave transformation modeling was performed for high, mean and low water levels to incorporate the effect of water level changes in the shallow water wave hindcasts. The water depth time series measured by the CDIP pressure sensor array were examined for the period 03/30/89 to 12/20/96, to compute the measured mean water depth and maximum and minimum depths. These were used to compute the water level variations at Imperial Beach during the time of the measurements and define the corresponding water levels, referred to MLLW, for input in the wave transformation model. Table 4 shows the maximum, mean and minimum water levels at Imperial Beach, referred to MSL and MLLW. The difference of 0.90 m between the MSL and MLLW at San Diego, just North of Imperial Beach, was used to refer the measured levels to MLLW.

	Depth (m)	Water Level (m)	
		(MSL)	(MLLW)
Maximum	11.93	1.51	2.40
Mean	10.42	0.00	0.90
Minimum	8.99	-1.43	-0.53

Table 4. Water depths and levels for Imperial Beach, from 03/30/89 to 12/20/96.

5. MODELING RESULTS

The deep water wave conditions summarized in Table 1 resulted in seas and swell matrices of 165 seas conditions (5 periods, 11 directions and 3 water levels) and 168 swell conditions (7 periods, 8 directions and 3 water levels), that were independently modeled with a unit significant wave height (Hs = 1). The modeling effort produced corresponding matrices of the wave transformation coefficient, Ct, and mean wave direction, MWD, at the location of the CDIP pressure sensor array measurements. Note that the Ct's and MWD's in the results matrices are average values over an area of approximately 200 m^2 covering several grid points and centered at the CDIP pressure array location.

Table 5 through Table 8 show the results of the wave transformation modeling for MSL.

Deep Water MWD	Tp (sec)								
	2	3	4	5	6	7	8	9	10
240	0.99	0.96	0.92	0.89	0.86	0.83	0.81	0.78	0.76
250	1.00	0.97	0.95	0.91	0.88	0.85	0.83	0.81	0.78
260	1.00	0.97	0.94	0.92	0.89	0.86	0.84	0.83	0.81
270	1.00	0.96	0.94	0.93	0.90	0.87	0.85	0.84	0.82
280	1.00	0.99	0.96	0.93	0.90	0.88	0.86	0.84	0.82
290	1.00	0.95	0.92	0.87	0.84	0.82	0.81	0.80	0.79
300	0.97	0.89	0.85	0.80	0.76	0.74	0.73	0.72	0.71
310	0.94	0.84	0.75	0.68	0.64	0.61	0.61	0.61	0.61
320	0.72	0.64	0.58	0.54	0.50	0.48	0.47	0.48	0.49
330	0.55	0.50	0.46	0.42	0.37	0.36	0.34	0.34	0.34

Table 5. Ct at MSL for seas.

Deep Water MWD	Tp (sec)								
	2	3	4	5	6	7	8	9	10
240	201	215	225	234	240	245	247	249	251
250	230	237	242	247	251	254	257	260	260
260	269	267	265	265	266	267	268	268	268
270	270	270	271	272	272	273	273	273	273
280	270	273	276	278	279	279	278	278	278
290	295	293	292	291	289	287	285	283	281
300	299	298	297	295	293	290	288	286	284
310	303	300	300	298	296	294	291	289	286
320	305	304	303	301	299	297	294	291	288
330	310	308	306	305	302	300	296	294	290

Table 6. MWD at MSL for seas.

Deep Water MWD	Tp (sec)								
	8	10	12	14	16	18	20	22	24
200	0.30	0.29	0.29	0.35	0.51	0.64	0.60	0.62	0.66
210	0.44	0.42	0.40	0.48	0.59	0.64	0.60	0.61	0.62
220	0.56	0.56	0.56	0.64	0.68	0.65	0.59	0.56	0.54
230	0.63	0.69	0.73	0.77	0.75	0.70	0.65	0.61	0.56
240	0.78	0.79	0.81	0.77	0.73	0.72	0.73	0.72	0.71
250	0.78	0.80	0.82	0.83	0.86	0.92	0.92	0.94	0.95
260	0.79	0.79	0.80	0.82	0.86	0.88	0.92	0.96	0.97
270	0.84	0.81	0.78	0.79	0.86	0.91	0.95	0.97	0.99
280	0.84	0.84	0.85	0.85	0.86	0.89	0.95	0.96	0.98
290	0.84	0.86	0.88	0.93	0.98	1.02	1.04	1.05	1.07
300	0.66	0.73	0.80	0.85	0.94	1.02	1.10	1.17	1.25
310	0.56	0.61	0.67	0.71	0.77	0.88	1.00	1.13	1.23
320	0.46	0.51	0.59	0.60	0.63	0.76	0.86	1.01	1.14

Table 7. Ct at MSL for swell.

Deep Water MWD	Tp (sec)								
	8	10	12	14	16	18	20	22	24
200	240	247	253	258	261	263	264	264	265
210	244	250	255	259	262	263	264	265	265
220	250	254	258	261	263	264	265	265	265
230	254	257	260	262	264	265	266	266	266
240	257	260	263	264	265	266	267	267	267
250	261	264	266	267	268	268	269	269	269
260	268	269	269	270	270	270	270	271	271
270	273	273	272	272	271	271	271	271	271
280	278	277	276	275	274	274	273	273	273
290	283	281	279	277	277	276	275	275	275
300	287	285	282	279	278	277	277	277	276
310	290	287	284	282	280	279	278	277	276
320	293	289	286	284	281	280	279	278	276

Table 8. MWD at MSL for swell.

With the objective of expanding the range of conditions for the transfer functions, results were extrapolated to conditions not covered in Table 1. The extrapolated values are shown shaded in Table 5 through Table 8. These "tails" were defined by just continuing the trends within the results matrices. Note that for a couple of cases there are shaded results within the swell results matrices. These are results produced by the model which were considered questionable and were therefore interpolated using neighboring points.

Table 9 through Table 12 show the effect of water level variations on Ct and MWD for seas and swell. Values reported in these Tables are the relative differences, for corresponding pairs in the matrices, computed by:

$$\Delta Ct = \frac{\left(Ct_{MHHW} - Ct_{MLLW}\right)}{Ct_{MLLW}} x\,100 \qquad (8)$$

and

$$\Delta MWD = MWD_{MHHW} - MWD_{MLLW} \qquad (9)$$

Deep Water MWD	Tp (sec)				
	5	6	7	8	9
250	3%	3%	4%	2%	1%
260	4%	5%	2%	2%	1%
270	3%	2%	2%	1%	1%
280	2%	2%	1%	0%	0%
290	4%	2%	2%	0%	-1%
300	4%	3%	3%	1%	-1%
310	6%	6%	5%	2%	-2%
320	6%	6%	4%	2%	0%

Table 9. ΔCt for seas.

MWD	10	12	14	16	18	20	22
210	13%	5%	-8%	-5%	-2%	2%	-3%
220	5%	-2%	-3%	0%	-2%	0%	-7%
230	1%	-1%	-4%	-3%	-4%	-3%	-5%
240	0%	-1%	0%	-3%	-3%	-3%	-3%
250	0%	-1%	-1%	-1%	-3%	0%	-4%
260	-1%	-4%	-5%	-6%	-5%	-5%	
270	1%	0%	-1%	-2%	-4%	-4%	-4%
280	0%	-1%	0%	1%	0%	-1%	-3%
290	-3%	-3%	-4%	-4%	-3%	-1%	0%
300	-4%	-5%	-6%	-6%	-6%	-5%	
310	-5%	-6%	-4%	-8%	-9%	-9%	-8%

Table 10. ΔCt for swell.

Deep Water MWD	Tp (sec)				
	5	6	7	8	9
250	-1	-2	-2	-3	-3
260	-2	-2	-2	-3	-2
270	-1	-1	-1	-1	-1
280	0	-1	-1	0	0
290	0	0	0	0	0
300	1	1	1	1	1
310	1	2	2	2	2
320	1	2	2	2	2

Table 11. ΔMWD (deg) for seas.

Deep Water MWD	Tp (sec)						
	10	12	14	16	18	20	22
210	-7	-6	-5	-3	-3	-4	-4
220	-6	-5	-4	-4	-3	-3	-3
230	-5	-4	-4	-3	-3	-3	-3
240	-4	-3	-3	-3	-3	-3	-3
250	-2	-2	-2	-2	-2	-2	-2
260	-2	-2	-2	-2	-2	-2	
270	-6	-5	-4	-3	-3	-3	-3
280	-1	-1	-1	-1	-1	-1	-1
290	0	0	0	-1	-1	-1	0
300	1	1	0	0	-1	0	
310	2	1	1	1	0	0	0

Table 12. ΔMWD (deg) for swell.

Table 9 and Table 10 suggest that the effect of water level variation is small for wave heights while Table 11 and Table 12 suggest that the effect on shallow water wave direction may or may not be important, depending on the kind of problem the resulting wave data will be used for. For example, 2 to 3 degrees difference in wave angle of incidence will not be important in ship seakeeping studies or design of structures, but it may be significant in sediment transport studies. Since the main objective of this study was to perform an overall comparison of wave parameters only Ct's and shallow water MWD's at

MSL where considered in the derivation of the transfer functions.

Three-dimensional B-spline interpolation was applied to the matrices of results to define continuous transfer functions that allowed the computation of seas and swell conditions at the CDIP pressure sensor array location for any arbitrary deep water wave height, period and direction within the conditions described in Table 5 through Table 8, and water levels within the range listed in Table 4. These functions were applied to each point of the deep water hindcast to compute the shallow water wave hindcast, at each 3-hour time interval, over the period from 1983 to 1996. Figure 2 through Figure 9 show the transfer functions.

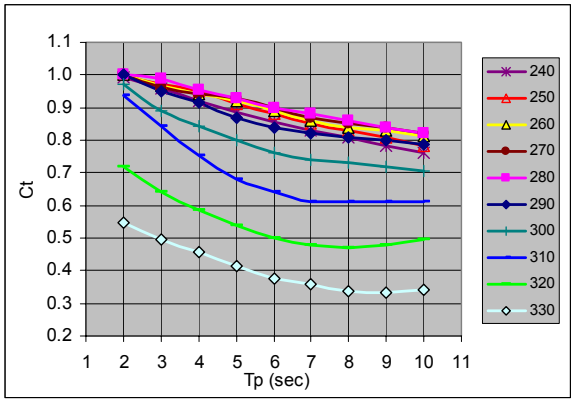

Figure 2. Ct versus Tp for seas at MSL, for a range of deep water MWD.

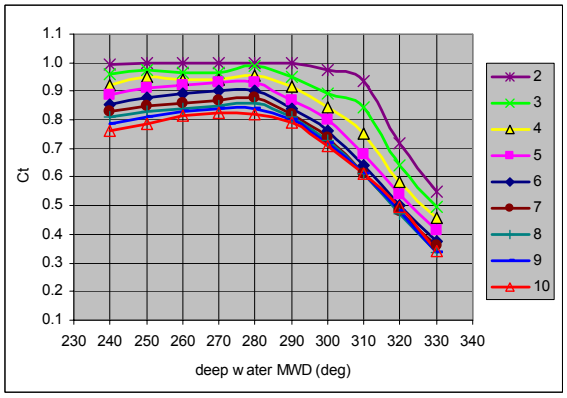

Figure 3. Ct versus deep water MWD for seas at MSL, for a range of Tp.

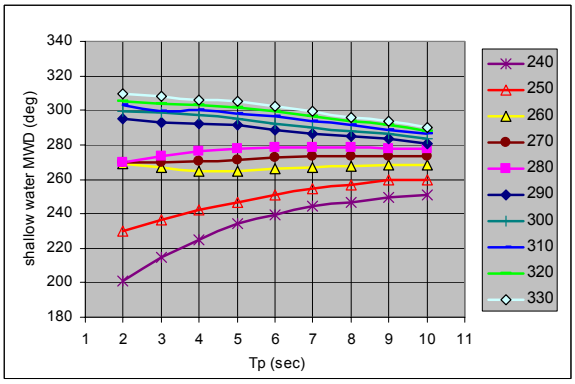

Figure 4. Shallow water MWD versus Tp for seas at MSL, for a range of deep water MWD.

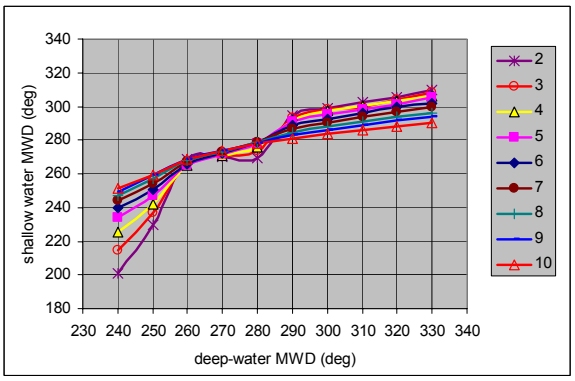

Figure 5. Shallow water MWD versus deep water MWD for seas at MSL, for a range of Tp.

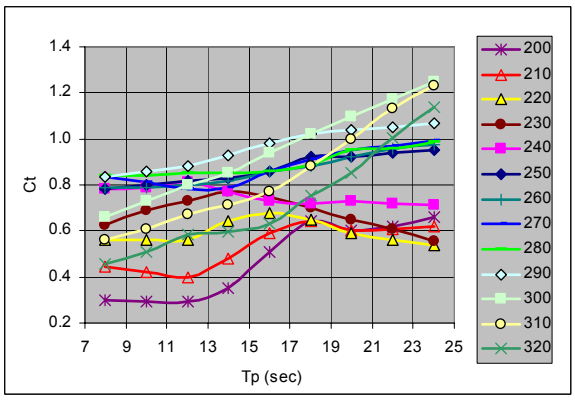

Figure 6. Ct versus Tp for swell at MSL, for a range of deep water MWD.

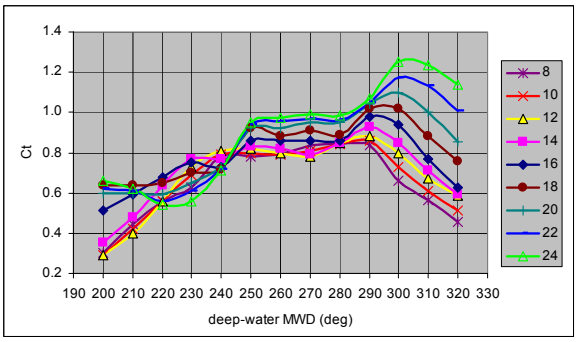

Figure 7. Ct versus deep water MWD for swell at MSL, for a range of Tp.

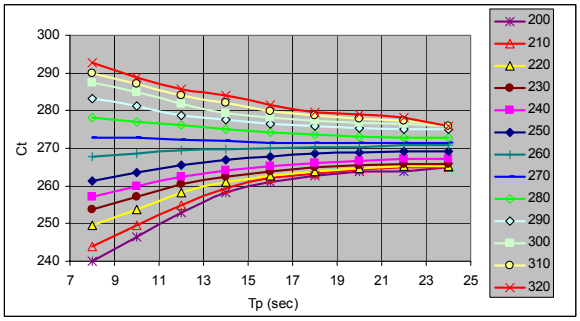

Figure 8. MWD versus Tp for swell at MSL, for a range of deep water MWD.

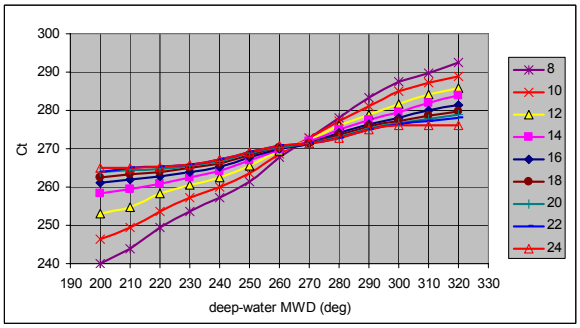

Figure 9. MWD versus deep water MWD for swell at MSL, for a range of Tp.

6. SHALLOW WATER WAVE HINDCASTS

The transfer functions derived from the results shown in Table 5 through Table 8 were computed with a three-dimensional B-spline routine. The first step in the derivation of the transfer functions was the computation of spline knots and coefficients which were later used to evaluate conditions within the wave conditions defined in Table 1 and the neighboring conditions defined by extrapolation. The significant advantage of fitting data with splines over other methods is that it does not produce undesirable wiggles away from the data points.

The transfer functions developed to compute the wave conditions at the location of the CDIP pressure sensor array do not have an analytical form. Instead, they are defined by spline knots and coefficients which are loaded by a spline evaluation routine. The routine uses the period and deep water MWD (and water level when applicable) to obtain the corresponding Ct or MWD at the location of interest. These parameters are computed according to Eq. (1) and Eq. (3).

The shallow water seas and swell hindcasts were computed, at every time interval on a point by point basis, operating on the deep water hindcast. Given the deep water Hs, Tp, MWD and water level, the corresponding wave height and mean wave direction at the CDIP pressure array were computed according to Eqs. (2) and (3). The criteria described in Table 13 and Table 14 were used to compute conditions outside the ranges of the transfer functions and to account for those cases where the deep water wave direction was "from land".

Seas Parameters ($Tp_{shallow\ water} = Tp_{deep\ water}$)		
Shallow Water		***Deep Water**
MWD	= f(240˚, Tp),	if MWD < 240˚
	= f (330˚, Tp),	if MWD > 330˚
H	= H^* x f(240˚, Tp)	if 180˚ < MWD < 240˚
	= 0	if 330˚ < MWD ≤ 360˚
	= 0	if 0˚ ≤ MWD ≤ 180˚

Table 13. Criteria to compute shallow water seas conditions for deep water wave conditions not defined by the transfer function.

Swell Parameters ($Tp_{shallow\ water} = Tp_{deep\ water}$)		
Shallow Water		***Deep Water**
MWD	= f (200˚, Tp),	if MWD < 200˚
	= f (320˚, Tp),	if MWD > 320˚
H	= H^* x f(200˚, Tp)	if 180˚ < MWD < 200˚
	= H^* x f(320˚, Tp)	if 320˚ < MWD < 330˚
	= 0	if 330˚ ≤ MWD ≤ 360˚
	= 0	if 0˚ ≤ MWD ≤ 180˚

Table 14. Criteria to compute shallow water swell conditions for deep water wave conditions not defined by the transfer function.

The total seas hindcast in shallow water were derived from the corresponding swell and seas hindcasts. For each point in the hindcast, the total significant wave height was computed according to Eq. (5).

The dominant peak period (Tp dominant) was defined as the one corresponding to the greater of the swell or seas wave height. For instance, if $H_{swell} > H_{seas}$ then Tp dominant = Tp swell, and viceversa. The dominant mean wave direction was computed similarly.

7. RESULTS

Detailed comparisons between time series of hindcast and measured wave heights, periods and mean wave directions are presented for selected storm periods. Figure 10 through Figure 12 show these parameters for March-May 1985.

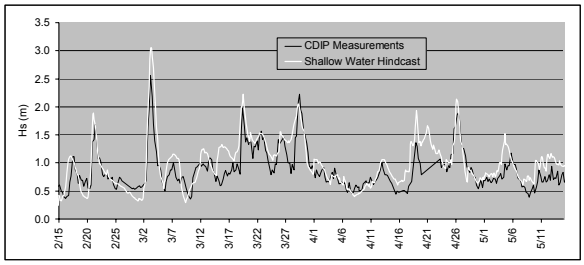

Figure 10. Measured and hindcast significant wave heights, Hs, for March-May 1985.

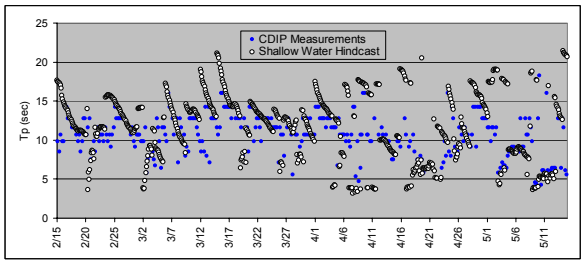

Figure 11. Measured and hindcast peak wave periods, Tp, for March-May 1985.

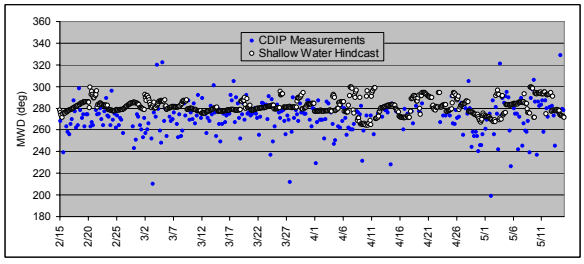

Figure 12. Measured and hindcast mean wave direction, MWD, for March-May 1985.

Figure 13 through Figure 15 show Hs, Tp and MWD for March-April 1987.

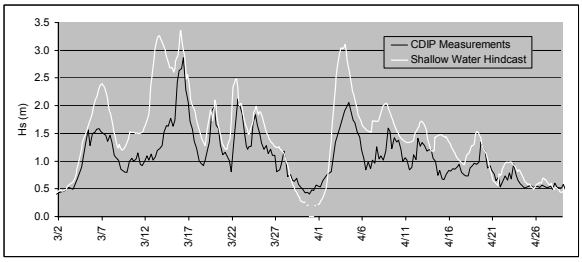

Figure 13. Measured and hindcast significant wave height, Hs, for March-April 1987.

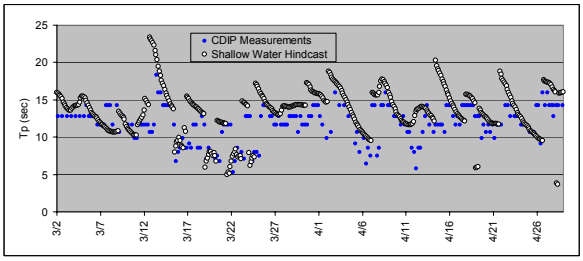

Figure 14. Measured and hindcast peak wave periods, Tp, for March-April 1987.

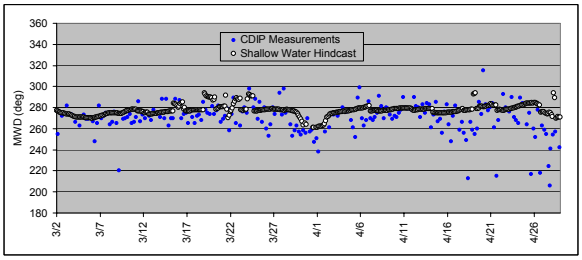

Figure 15. Measured and hindcast mean wave directions, MWD, for March-April 1987.

Figure 16 through Figure 18 show Hs, Tp and MWD for November-December 1990.

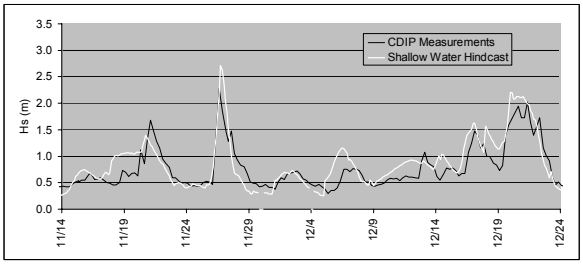

Figure 16. Measured and hindcast significant wave heights, Hs, for November-December 1990.

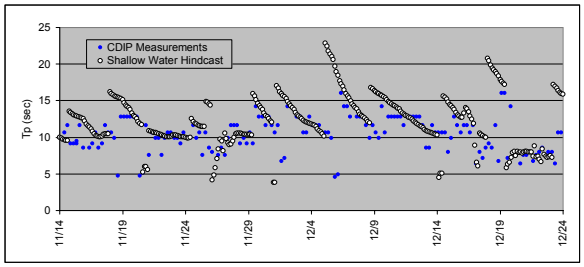

Figure 17. Measured and hindcast peak wave period, Tp, for November-December 1990.

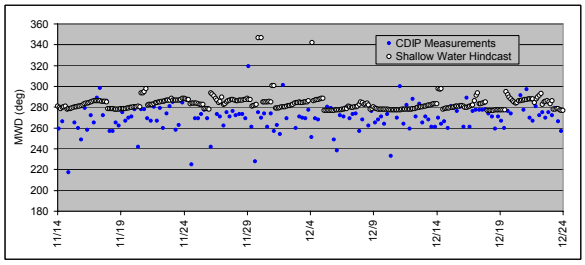

Figure 18. Measured and hindcast mean wave direction, MWD, for November-December 1990.

Figure 19 and Figure 20 show Hs and Tp (no MWD measurements available) for January-April 1991.

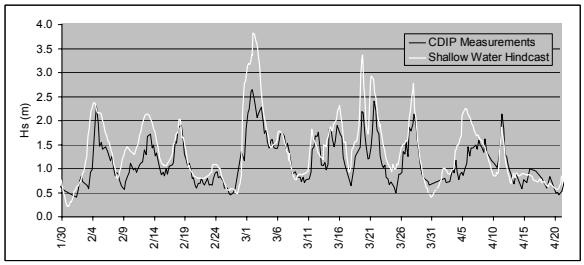

Figure 19. Measured and hindcast significant wave heights, Hs, for January-April 1991.

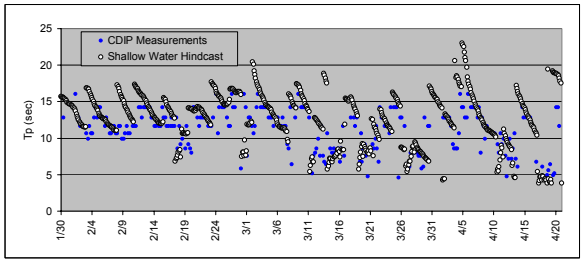

Figure 20. Measured and hindcast peak wave period, Tp, for January-April 1991.

Figure 21 and Figure 22 show Hs and Tp (no MWD measurements available) for November-December 1992.

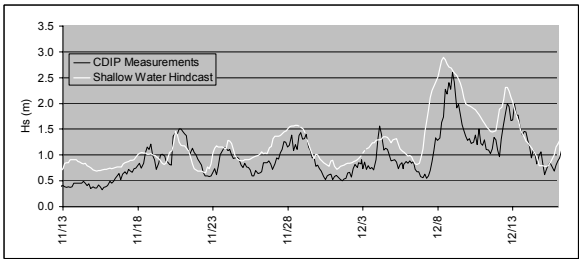

Figure 21. Measured and hindcast significant wave heights, Hs, for November-December 1992.

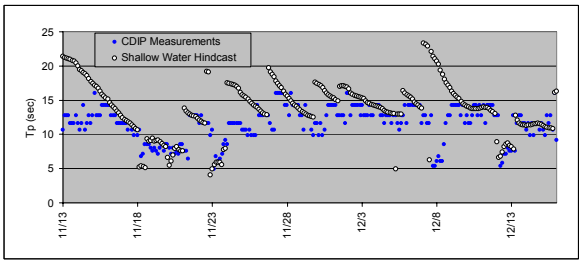

Figure 22. Measured and hindcast peak wave period, Tp, for November-December 1992.

Figure 23 and Figure 24 show Hs and Tp (no MWD measurements available) for January-March 1993.

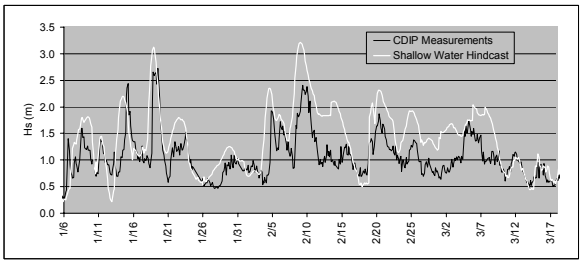

Figure 23. Measured and hindcast significant wave heights, Hs, for January-March 1993.

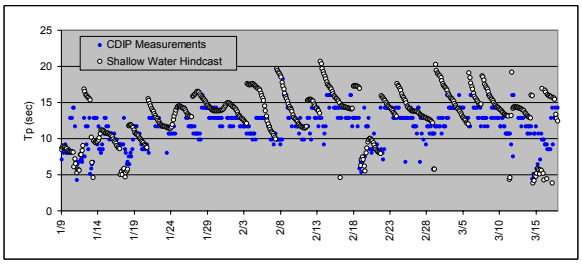

Figure 24. Measured and hindcast peak period, Tp, for January-March 1993.

Figure 25 and Figure 26 show Hs and Tp (no MWD measurements available) for March-May 1995.

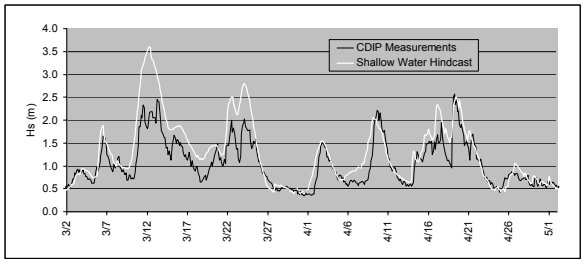

Figure 25. Measured and hindcast significant wave heights, Hs, for March-May 1995.

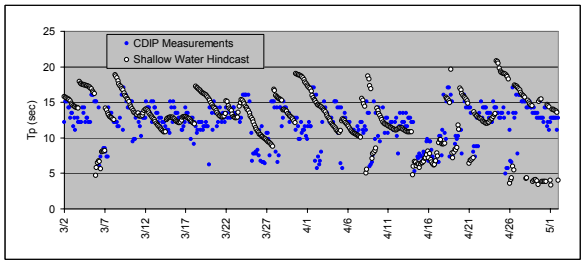

Figure 26. Measured and hindcast peak period, Tp, for March-May 1995.

Figure 27 and Figure 28 show Hs and Tp (no MWD measurements available) for October-December 1996.

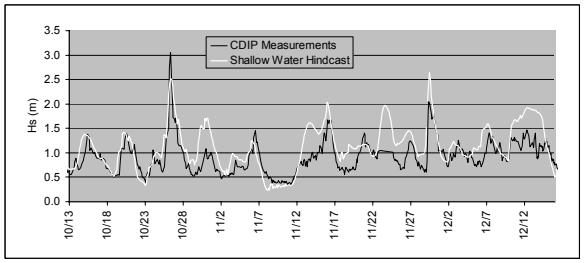

Figure 27. Measured and hindcast significant wave heights, Hs, for October-December 1996.

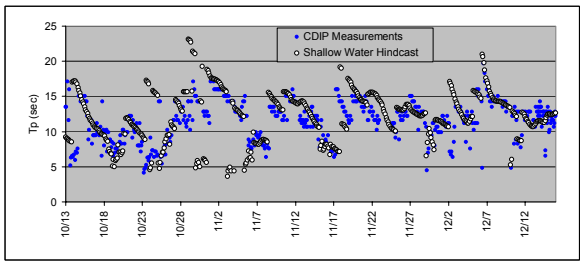

Figure 28. Measured and hindcast peak period, Tp, for October-December 1996.

7.1. Bias, Scatter Index and Cross-Correlation

CDIP data is available from 1983 to 1996. However, years 1983, 1986 and 1988 had large amounts of missing measurements. Therefore, only years 1984, 1985 and 1989 to 1996 were considered in this analysis. The derived shallow water hindcast and measurements did not have corresponding times, and therefore, the CDIP data was resampled so that times were coincident with those of the hindcast. Residuals of wave heights, the difference between the hindcast and measurements, were computed to derive the statistics typically used to quantify the discrepancies between measured and hincast wave heights. Figure 29 shows the bias (average of the residuals), Figure 30 the root-mean-squared error (RMS error, square root of the average of the residuals squared), Figure 31 the scatter index (SI, the ratio between the standard deviation of the residuals and the average of the measurements) and Figure 32 the cross-correlation coefficient (CC).

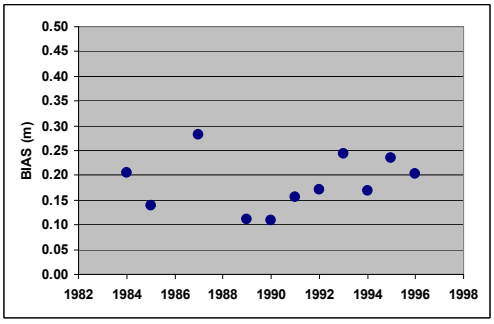

Figure 29. Bias for shallow water wave hindcast and CDIP measurements.

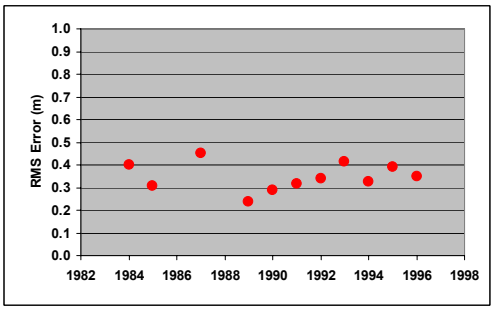

Figure 30. RMS error for shallow water wave hindcast and CDIP measurements.

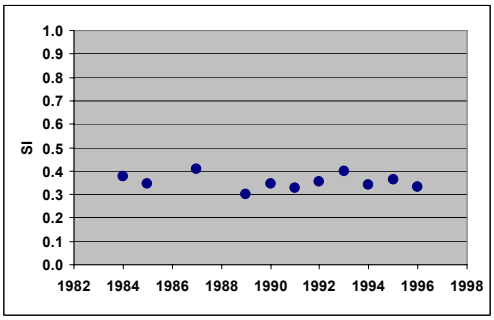

Figure 31. Scatter Index, SI, for shallow water wave hindcast and CDIP measurements.

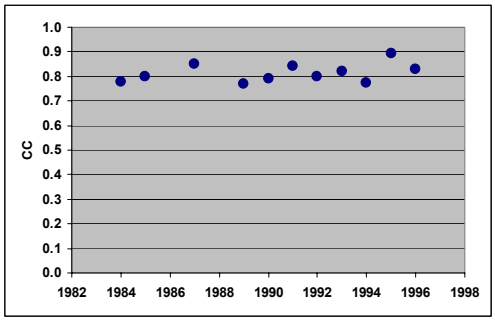

Figure 32. Cross-correlation coefficient, CC, between shallow water wave hindcast and CDIP measurements.

7.2. Quantile-Quantile Comparisons

Quantile-Quantile (Q-Q) comparisons for shallow water hindcast versus CDIP measured significant wave heights from 1983 to 1996 are shown in Figure 33.

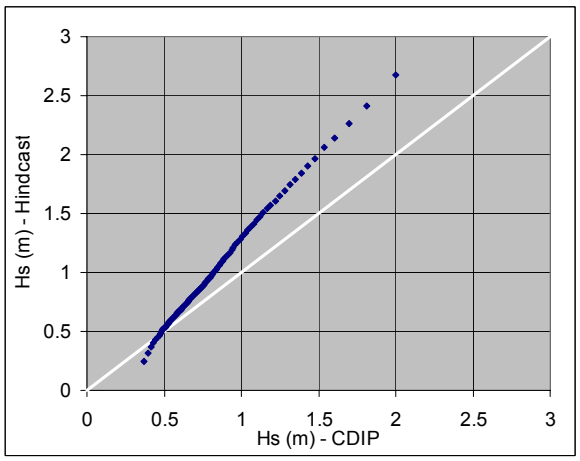

Figure 33. Q-Q (from 1 to 99%) for shallow water hindcast and CDIP measured significant wave heights from 1983 to 1996.

The Q-Q comparisons show a trend of the wave heights being overestimated by the shallow water hindcast.

8. DISCUSSIONS OF RESULTS

The analysis of the time series, statistics and Q-Q plot presented in the previous section indicate that, even thought the general features of the waves are matched, the shallow water wave hindcast is not consistent with the CDIP measurements, in particular during the relative high wave events. In order to explain the sources of the discrepancies, several aspects of the modeling that was performed were analyzed.

The outcome of a modeling effort is greatly dependent on a multitude of factors, which include the quality of the input and validation data, and the soundness of the assumptions made. This study was not intended to analyze the quality of the data and models used. The GROW hindcast, for example, has been validated extensively and cited in the literature. The wave transformation model used, MIKE 21 PMS developed by DHI, has been widely adopted and validated, within the limits of the theories implemented in the model. Since its inception in 1975, CDIP has been managing an extensive network for monitoring waves along the coastlines of the United States. CDIP routinely implements rigorous quality controls at several stages in the data processing to provide users with quality data.

The selection of the wave hindcast at GROW station 38023 was based on its close proximity to Imperial Beach and on its location in deep water (depth = 1,000 m). This station accounts for basin and local scale events, as well as the sheltering effects of the islands in the California Bight. The impact on the resulting wave heights of selecting a different station, located further offshore, for the input wave conditions is difficult to determine. Waves from a station further offshore would be larger, but a larger and finer wave transformation model may account better for the sheltering effects of the nearby islands, resulting in smaller wave heights at Imperial Beach.

The wave transformation model did not account for dissipation due to wave-wave interaction and transformation due to wave-current interaction. In addition, no wind forcing was included. Bottom friction was included in the form of the Nikuradse roughness parameter $k_n = 2.5d_{50} = 0.002$, where d_{50} is the median grain size (m). However, since all waves were modeled with Hs =1 m, the effect of bottom friction was probably underestimated for the higher waves. Directional spreading and spectral shapes are parameters that are expected to change in time. The methodology presented in this paper adopted a simplified approach and assumed these constant (see Table 2). In order to evaluate the sensitivity of Ct on directional spreading and spectral shape a few model runs were performed. Changes in the order of 0 to 5% (depending on wave period and direction) were found, which would not be sufficient to explain the differences between the wave heights of the shallow water hindcast and the measurements. Finally, the bathymetry offshore Imperial Beach is quite complex featuring islands, shoals and submarine canyons. Discrepancies between the real and modeled bathymetries would be important since the wave transformation processes are controlled by changes in depth. Even though the bathymetry modeled was very detailed and believed to be derived from a good source, its accuracy is unknown and therefore a definite assessment of the impact of the bathymetry cannot be performed at this time. However, it is believed that the bathymetry used correctly

represented the general features of the area and that the computed negligible variation in Ct for the extreme maximum and minimum water levels suggest that the effect of the bathymetry in the results was minor (see Table 9 and Table 10).

The time series shown indicate discrepancies during events of high waves with long periods (i.e. Tp > 12 seconds) (see Figure 10 through Figure 28) and the Q-Q plot shows that discrepancies increase with wave height. The reasons why the shallow water hindcast produces larger waves than the measurements for high wave events are not readily apparent. However, it is important to recall that the CDIP waves were derived from pressure records transferred to surface elevation using Linear Wave Theory in the frequency domain. In the 10 m water depth range where the measurements were made, the larger waves are definitely in the non-linear range. Figure 34 shows the shallow water wave hindcast data in terms of wave steepness (H/Lo) and relative water depth (d/Lo), Linear Wave Theory limits (SPM, 1984) and Stream Function Theory limits (H/Hb, where Hb = breaking wave height) (Dean, 1974).

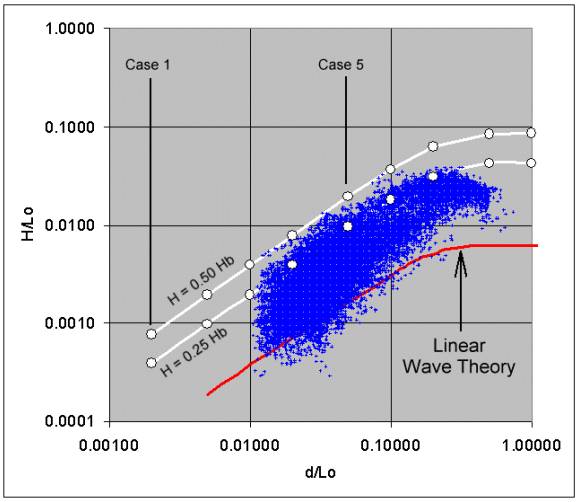

Figure 34. Shallow water hindcast, Stream Function and Linear Wave Theory limits.

It can be seen in Figure 34 that the majority of the waves fall outside the Linear Wave Theory limit and many of the larger waves are in the range of 25 to 50% of the limit breaking wave height. In the Stream Function Wave Theory, the latter correspond to Cases A-3 to 7 (H/Hb = 25%) and Cases B-3 to 7 (H/Hb = 50%). Figure 35 shows the storm peak wave heights shown in the time series presented in Section 7, for which H > 2.5 m.

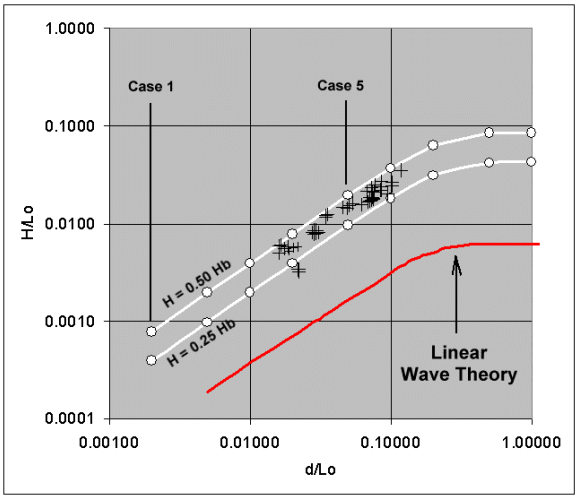

Figure 35. Storm peak wave heights from time series shown in Section 7, H > 2.5 m.

Pressure records do not reproduce exactly the water surface elevation above them, but represent instead an attenuated version. It is possible to recover water surface elevation from pressure records if the appropriate transfer function is known. The development of such transfer function has been the objective of many studies and the suitability of the various ones derived has been the focus of debate for many years. In principle, the water surface elevation, η, could be derived according to:

$$\eta = \frac{p}{\rho g K_p} \tag{10}$$

where p is the dynamic pressure, g is the acceleration due to gravity and K_p is the transfer function.

The transfer function based on Linear Wave Theory is the simplest one of all and more widely used. It relates dynamic pressure with water surface elevation, for a pressure sensor on the bottom, according to the following equation:

$$K_p = \frac{1}{\cosh\left(\frac{2\pi}{L} d\right)} \tag{11}$$

where L is the shallow water wave length and d is the water depth.

The fact that the water surface elevation or wave heights cannot be predicted correctly solely on the basis of Linear Wave Theory has been shown by many investigators (Seiwell, 1947; Draper, 1957; Glukhovskiy, 1961, Hom-ma., 1966; Bergan, 1968; Grace, 1978; Cavaleri, 1980; Forristall, 1982; Biesel, 1982; Lee, 1984 and Kuo, 1994). In order to compensate for the discrepancies found in their studies

investigators introduced an empirical factor N which was implemented in Eq. (10) as follows:

$$\eta = N \frac{p}{\rho g K_p} \qquad (12)$$

Eq. (10), (11) and (12) have been applied in the frequency domain to extend the applicability of the transfer function to irregular waves. However, Grace (1978) and Nielsen (1986) have pointed out that, in shallow water cases, the harmonics present in the shallow-trough and peaked-crest waves are not dispersive and therefore the application of Eq. (11) to these waves is not proper This argument has lead to "wave-by-wave" analysis methods which also showed discrepancies between predicted and measured waves.

The factors that affect N, such as relative water depth, wave steepness, sensor elevation current, noise, etc. have been investigated by means of laboratory tests and field experiments with both frequency domain and "wave-by-wave" methods. Despite the extensive investigations, how these factors affect N is not clearly understood and useful relationships are still required. Nevertheless, the bulk of the literature cited above suggests that corrections to Eq. (10) are required and essential in shallow water wave conditions. Constant or functional relationships of N have been suggested with values of N in the range of $1 \leq N \leq 1.35$.

An assessment of the potential error of wave heights derived from pressure measurements can be performed by comparing wave heights resulting from more precise non-linear wave theories, such as the Stream Function Wave Theory, and those derived using the Linear Wave Theory transfer function K_p. For the water depth at Imperial Beach (d =10.42 m), Table 15 and Table 16 show the relative error for H/Hb = 0.25 and H/Hb = 0.50, respectively. The dynamic pressure head, $p/\rho g$, was computed, according to the Stream Function Wave Theory, for each case.

		Cases				
	Units	3	4	5	6	7
d/Lo	-	0.01	0.02	0.05	0.1	0.2
H/Lo	-	0.0019	0.0039	0.0098	0.0183	0.0313
Lo	m	1042	521	208.4	104.2	52.1
T	sec	25.8	18.3	11.6	8.2	5.8
H	m	2.03	2.03	2.03	1.91	1.63
$p/\rho g$	m	1.77	1.76	1.66	1.33	0.75
Kp	-	0.969	0.938	0.847	0.705	0.459
$H_{\text{Linear Wave}}$	m	1.83	1.88	1.95	1.88	1.64
$(H_{\text{Linear Wave}} - H) / H$		-10%	-8%	-4%	-1%	1%

Table 15. Relative error of wave height derived with Linear Wave Theory transfer function and Stream Function Wave Theory for H/Hb = 0.25.

		Cases				
	Units	3	4	5	6	7
d/Lo	-	0.01	0.02	0.05	0.1	0.2
H/Lo	-	0.0039	0.0078	0.0195	0.0366	0.0625
Lo	m	1042	521	208.4	104.2	52.1
T	sec	25.8	18.3	11.6	8.2	5.8
H	m	4.05	4.05	4.06	3.82	3.26
$p/\rho g$	m	3.14	3.11	3.02	2.54	1.53
Kp	-	0.969	0.938	0.847	0.705	0.459
$H_{\text{Linear Wave}}$	m	3.24	3.32	3.56	3.61	3.33
$(H_{\text{Linear Wave}} - H) / H$		-20%	-18%	-12%	-6%	2%

Table 16. Relative error of wave height derived with Linear Wave Theory transfer function and Stream Function Wave Theory for H/Hb = 0.50.

The wave period comparisons show good agreement in general. However, the measured periods, which are clustered in discrete bands because they are derived from wave spectra, rarely exceeded 16 seconds. The probability distributions of Tp for the shallow water wave hindcast and measurements are shown in Figure 36.

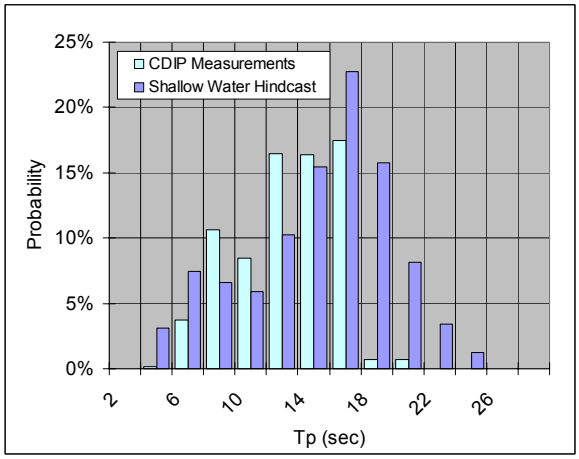

Figure 36. Probability distributions of Tp for shallow water wave hindcast and CDIP measurements.

The reasons why the measurements show higher probabilities of Tp towards the shorter periods than the shallow water hindcast are not readily apparent. However, it may be due to the fact that, in the transfer of pressures to surface waves with K_p (Eq. (11)) the shorter periods are given more weight. The measured pressures are attenuated at the seafloor and, as seen in Table 15 and Table 16, K_p tends to underestimate the long period waves and overestimate the short period ones, shifting the spectral peaks to the shorter periods. The shallow water wave hindcast shows the expected phenomena of waves of longer periods arriving first, as a storm approaches, followed by waves of shorter periods as the wave heights increase.

The wave direction predictions show the expected

alignment with the general orientation of the coastline. The measurements appear more "noisy" and preclude any conclusion about the accuracy of the predictions.

9. CONCLUSIONS

The methodology presented in this paper constitutes a simple methodology for the derivation of long-term hindcasts in shallow water including the particular features of the nearby bathymetry. Provided that a global long-term hindcast is used, the resulting shallow water hindcast would include basin and local scale events.

The various assumptions made for the wave transformation modeling seem adequate, in particular those made for the spectral and directional spreading characteristics of Pacific Ocean seas and swell.

The overall agreement of the shallow water wave hindcast with the measurements is good, following the general features of the measurements. The agreement is very good for smaller wave height, shorter period waves, but the hindcast is not consistent with the measurements for the high and long period waves. The latter has been attributed to the inherent limitations of the Linear Wave Theory transfer function used in the derivation of wave heights from pressure measurements. The statistics presented, which are typically used to characterize the discrepancies between hindcasts and measurements, should be evaluated keeping in mind that a review of the literature and comparisons between Linear and Stream Function Wave Theories pressure-to-wave-height transfer functions revealed that height corrections to the measurements could be in the range of 0 to 30%.

10. ACKNOWLEDGEMENTS

The author wishes to thank Vincent Cardone and Oceanweather, Inc. for providing the deep water wave hindcast used in this study and for the valuable comments and suggestions. The assistance and guidance of Dr. J. Ian Collins is gratefully acknowledged.

11. REFERENCES

Arthur, R.S., 1951: Wave forecasting and hindcasting. Proceedings of the 1st International Conference on Coastal Engineering, Chapter 8, 82-87.

Bergan, P.O., Torum, A. and Traetteberg, A., 1968: Wave measurements by a pressure type wave gauge. Proceedings of the 11th International Conference on Coastal Engineering, Chapter 3, 19-29.

Biesel, F., 1982: Second order theory of manometer wave measurement. Proceedings of the 18th International Conference on Coastal Engineering, Vol. 1, 129-135.

Cavaleri, L., 1980: Wave measurement using pressure transducer. Oceanologia Acta, 3, 3, 339-346.

Dean, R.G. 1974: Evaluation and Development of Water Wave Theories for Engineering Application. US Army Corps of Engineers, Coastal Engineering Research Center, Vol. 1 and 2.

Draper, L., 1957: Attenuation of sea waves with depth. La Houille Blanche, Vol. 21, No. 6.

Forristall, G.Z., 1982: Subsurface wave measuring systems. Proceedings of a Symposium and Workshop on wave measurement technology. Marine Board of the National Research Council, 194-209.

Global Reanalysis of Ocean Waves (GROW). Project Description. Oceanweather, Inc.

Glukhovskiy, B.K.H., 1961: Study of wave attenuation with depth on the basis of correlation analysis. Meteorologiya i Gidrologiya, No. 11.

Goda, Y., 1985: Random Seas and Design of Maritime Structures. University of Tokyo Press.

Grace, R.A., 1978: Surface wave heights from pressure records. Coastal Engineering, 2, 55-67.

Hom-ma, M., Horikawa, K. and Komori, S., 1966: Response characteristics of underwater wave gauge. Proceedings of the 10th International Conference on Coastal Engineering, Chapter 8, 99-113.

Inman, D.L., 1974: Nearshore Processes Along the Silver Strand Littoral Cell. Intersea Research Corp., August 15, 1974.

Kuo, Y.Y. and Chiu, Y.F, 1994: Transfer function between wave height and wave pressure for progressive waves. Coastal Engineering, 23, 81-93.

Lee, D.Y. and Hsiang, W., 1984: Measurement of surface waves from subsurface gage. Proceedings of the 19th International Conference on Coastal Engineering, 271-286.

Nielsen, P., 1986: Local approximations: A new way of dealing with irregular waves. Proceedings of the 20th International Conference on Coastal Engineering, 633-646.

Seiwell, H.R., 1947: Investigation of underwater pressure records and simulteneous sea surface patterns. Transactions, American Geophysical Union, Vol. 28, No. 5, 722-724.

Shore Protection Manual, 1974. US Army Corps of Engineers. Coastal Engineering Research Center.